Work Order No. WO#582-16-61842-13
Contract # 582-15-50417
Tracking No. 2016-17

Final Report
Improved Halogen Chemistry for CAMx Modeling

PREPARED UNDER A CONTRACT FROM THE
TEXAS COMMISSION ON ENVIRONMENTAL QUALITY

The preparation of this report was financed through a contract from the State of Texas through the Texas Commission on Environmental Quality. The content, findings, opinions and conclusions are the work of the author(s) and do not necessarily represent findings, opinions or conclusions of the TCEQ.

Prepared for:
Jim Smith
Texas Commission on Environmental Quality
121 Park 35 Circle MC 164
Austin, TX 78753

Prepared by:
Christopher Emery, Zhen Liu,
Bonyoung Koo, Greg Yarwood
Ramboll Environ US Corporation
773 San Marin Drive, Suite 2115
Novato, California, 94945
www.ramboll-environ.com
P-415-899-0700
F-415-899-0707

May 2016

06-35854M

RAMBOLL ENVIRON

CONTENTS

1.0 INTRODUCTION 1

1.1 Background 1

1.2 Purpose and Objectives 2

2.0 OZONE DEPENDENT IODINE EMISSIONS 4

2.1 Science Background 4

2.1 CAMx Implementation 5

3.0 IODINE MECHANISM CONDENSATION 8

3.1 Sensitivity Analysis of Iodine Reactions 8

3.1.1 Model Description 8

3.1.2 Results and Discussion 8

3.2 Compact Iodine Mechanism 16

4.0 TESTING AND EVALUATION 18

4.1 CAMx Tests 18

4.1.1 Comparison of Ozone Impacts from Halogen Mechanisms 20

4.1.2 CAMx Speed Performance 21

4.2 CAMx Code Delivery 22

4.3 Running CAMx with Condensed Halogen Chemistry 22

4.3.1 Ozone Column File 23

5.0 CONCLUSION 26

6.0 REFERENCES 28

TABLES

Table 2-1(a). Aqueous iodide concentration [I^-_{aq}] and I_2, HOI and total Ix emission fluxes (Ix = HOI + 2×I_2) estimated using the parameterizations described by Prados-Roman et al. (2015) for surface ozone concentration of 40 ppb and wind speed of 3 m/s. 6

Table 2-1(b). As in Table 2-1(a), but for wind speed of 1 m/s. 6

Table 2-1(c). As in Table 2-1(a), but for wind speed to 5 m/s. 6

Table 3-1. Lists of reactions included in the full iodine mechanism (I-30), and in I-16b, I-16a and I-13 subgroups 17

Table 4-1. CAMx run times to simulate three days using three different chemical mechanisms on the 2006 TCEQ Rider 8 36/12 km grid system. 22

FIGURES

Figure 1-1. TCEQ 36/12/4 km CAMx nested modeling grids, from: http://www.tceq.texas.gov/airquality/airmod/rider8/modeling/domain 2

Figure 2-1. Annual mean Ix emission flux (nmol(Ix)/m^2/day) estimated by the CAM-Chem global chemistry-climate model, based on the parameterizations of Carpenter et al. (2013) and MacDonald et al. (2014). (From Figure 2 of Prados-Roman et al., 2015)..... 5

Figure 2-2. Estimated Ix emissions in the TCEQ 12 km modeling grid on June 18, 2006 in units of nmol(Ix)/m^2/day. The "offline" plot shows emissions generated by the SEASALT processor assuming uniform emissions at 1148 nmol(Ix)/m^2/day. The "in-line" plots show emissions generated within CAMx according to the equations of Prados-Roman et al. (2015). Note the difference in color scale for "in-line I_2"..... 7

Figure 3-1. 24-hour average O_3 sensitivity to rate constants of individual (or groups of) reaction(s), with $E(I_2)$ = 25 nmol m^2 hr^{-1}. Reactions shown in orange and tagged with "**" are those included in the 'I16b' compact iodine mechanism. 10

Figure 3-2. Schematic of the full iodine chemistry mechanism (I-30) in CB6r2h..... 11

Figure 3-3. 24-hour average of (a) change in O_3 as a function of I_2 emissions, (b) O_3 sensitivity to I_2 emissions, (c) I_XO_Y sensitivity to I_2 emissions, and (d) sensitivity of O_3 to I_XO_Y ($\partial[O_3]/\partial[I_XO_Y]$), at different I_2 emission fluxes. 13

Figure 3-4. Same as Figure 3-1, but with $E(I_2)$ = 10 nmol m^2 hr^{-1}. 14

Figure 3-5. Same as Figure 3-1, but with $E(I_2)$ = 1 nmol m^2 hr^{-1}. 15

Figure 4-1. CAMx vertical layer structure for the Rider 8 model of June 2006. TCEQ figure from http://www.tceq.texas.gov/airquality/airmod/rider8/modeling/domain 19

Figure 4-2. Changes in simulated MDA8 ozone on June 18, 2006 from three halogen mechanisms: CB6r2h (top left), I-30 (middle), and I-16b (right). Top panels show MDA8 ozone decrements relative to a no-halogen case using the standard CB6r2 mechanism, while the bottom panels show decrements resulting from I-30 and I-16b relative to the full halogen case (CB6r2h)..... 20

Figure 4-3. Time series at four coastal Gulf sites of hourly ozone reduction over June 17-18, 2006 from three halogen mechanisms: CB6r2h (red), I-30

(orange), and I-16b (blue). Ozone decrements are relative to a no-halogen case using the standard CB6r2 mechanism. 21

Figure 4-4. Example structure of a single-grid ozone column input file showing panels for the optional time-invariant land-ocean mask and time-varying ozone column field. 25

1.0 INTRODUCTION

1.1 Background

The Texas Commission on Environmental Quality (TCEQ) is responsible for developing the Texas State Implementation Plan (SIP) to demonstrate compliance with the National Ambient Air Quality Standard (NAAQS) for ozone. In 2015, the ozone NAAQS was recently lowered to 70 parts per billion (ppb) based on the three year running average of the annual fourth highest daily maximum 8-hour average (MDA8) ozone measured at each monitoring location. The ozone concentration in background air entering Texas may be as low as 10 ppb for clean air from the Gulf of Mexico or may approach the level of the NAAQS for air of continental origin. Correctly characterizing background ozone is very important to SIP planning because over-estimating background may indicate deeper local emission reductions than are actually needed to meet the NAAQS.

The TCEQ uses the Comprehensive Air Quality Model with extensions (CAMx; Ramboll Environ, 2016) for ozone SIP modeling. The TCEQ CAMx modeling domain covers most of the Gulf of Mexico (Figure 1-1). CAMx modeling for Texas is strongly affected by ozone over predictions in air arriving along the Texas coast (Smith et al., 2014). Ozone predictions along the coast depend upon emissions and chemistry over the Gulf of Mexico and boundary conditions entering the modeling domain. CAMx boundary conditions are derived from a global model (such as GEOS-Chem; Harvard, 2016), which also tends to over predict ozone in the Gulf region, as do many other regional and global models (Yarwood et al., 2012).

Iodine compounds emitted from ocean waters such as the Gulf of Mexico can cause ozone depletion of several ppb per day within the marine boundary layer (Mahajan et al., 2010 and references therein). Iodine depletes ozone catalytically, meaning that a single iodine atom can destroy many ozone molecules (Chameides and Davis, 1980; Mahajan et al., 2009). Emissions of inorganic iodine compounds (I_2 and HOI) are caused by deposition of ozone to ocean waters (Carpenter et al., 2013), whereas emissions of organic iodine compounds result from biological processes (Carpenter, 2003). Field study data from Mahajan et al. (2010) show that bromine chemistry operates in synergy with iodine chemistry to double the rate of ozone depletion in the marine boundary layer. Emissions of organic bromine compounds also result from biological processes (Carpenter, 2003), while sea-salt aerosol produced by bubble bursting and wind shear at the ocean surface is the dominant source of inorganic bromine and chlorine (Sander et al., 2003).

Yarwood et al. (2012) first extended CAMx chemistry to model ozone depletion by marine iodine emissions. CAMx simulated roughly 5 ppb of ozone depletion over the Gulf of Mexico in tests using a constant I_2 emissions flux and spatially varying organic iodine emissions based on monthly satellite observations of chlorophyll. Yarwood et al. (2014) then added more comprehensive halogen chemistry for iodine, bromine and chlorine to the Carbon Bond version 6, release 2 (CB6r2) chemical mechanism. The resulting mechanism (referred to as CB6r2h) added 88 more reactions to the original 216 (41% increase) and 33 more transported species to the original 75 (44% increase). In the Gulf of Mexico, ozone reductions exceeded 6 ppb near

Figure 1-1. TCEQ 36/12/4 km CAMx nested modeling grids, from: http://www.tceq.texas.gov/airquality/airmod/rider8/modeling/domain.

the Texas coastline, mostly attributable to iodine. Yarwood et al. (2014) found that CAMx simulation times with CB6r2h about doubled over those for CB6r2, while TCEQ found increases in model run times of about 60% (Smith et al., 2015).

1.2 Purpose and Objectives

The goal of this project was to improve both speed and accuracy in modeling ozone transported into Texas from the Gulf of Mexico by: 1) implementing a condensed halogen mechanism; and 2) implementing an in-line emissions algorithm that incorporates recent findings on the feedback between ozone deposition to ocean waters and emission flux of iodine (Prados-Roman et al., 2015; Garland and Curtis, 1981).

In Section 2, we evaluate the emission algorithms for inorganic reactive iodine (Ix; specifically I_2 and HOI) recently implemented by Prados-Roman et al. (2015) in a global chemistry model. We incorporated the algorithm into CAMx as an in-line routine that responds to surface layer ozone concentration, wind speed and sea surface temperature. We describe results and compare to our previous assumption of constant I_2 emission rate from ocean waters.

In Section 3, we develop a compact iodine mechanism to model ozone depletion by halogens over the Gulf of Mexico. Previously, Yarwood et al. (2014) found that Ix emissions accounted

for the majority of the effect of halogens on ozone and so the main strategy for this task was to reduce the halogen reactions in CB6r2h to the minimum required number of iodine reactions.

Section 4 documents results from testing the updated CAMx model using the same June 2006 ozone model inputs as were used in the preceding study (Yarwood et al., 2014). Section 5 presents our conclusions and recommendations stemming from this project. We have delivered the updated CAMx source code to the TCEQ for installation and testing on the TCEQ computer system.

2.0 OZONE DEPENDENT IODINE EMISSIONS

We evaluate the emission algorithms for inorganic iodine that were recently implemented by Prados-Roman et al. (2015) into a global chemistry model. We incorporate the algorithm into CAMx as an in-line routine that responds to surface layer ozone (O_3) concentration, wind speed and sea surface temperature (SST). We describe results and compare to our previously assumed constant I_2 emission rate.

2.1 Science Background

Iodine oxide (IO) has been detected in the marine boundary layer (Alicke et al., 1999) leading to many studies attempting to identify the source of iodine compounds and related chemistry (Saiz-Lopez et al., 2012). Evidence for an abiotic iodine source has mounted since 2008 (see references in Prados-Roman et al., 2015), most recently suggesting that emissions of inorganic iodine (Ix), including hypoiodous acid (HOI) and molecular iodine (I_2), result from sea surface reactions with deposited O_3. Carpenter et al. (2013) and MacDonald et al. (2014) have developed parameterization for Ix emissions that depend upon surface O_3 concentration, wind speed and SST.

Prados-Roman et al. (2015) used the Community Atmospheric Model with Chemistry (CAM-Chem) global chemistry-climate model (Lamarque et al., 2012) to quantify ocean emissions of inorganic reactive iodine (Ix = HOI + 2×I_2) resulting from tropospheric O_3. They find that long term O_3 enhancement has increased Ix emissions and in turn accelerated chemical loss of O_3 over the oceans in a negative feedback loop. Following the parameterization developed by Carpenter et al. (2013), CAM-Chem estimates Ix emissions according to:

$$E(HOI) = [O_3] \times \left[4.15 \times 10^5 \left(\frac{\sqrt{[I^-_{aq}]}}{w} \right) - \left(\frac{20.6}{w} \right) - 2.36 \times 10^4 \sqrt{[I^-_{aq}]} \right]$$

$$E(I_2) = [O_3] \times [I^-_{aq}]^{1.3} \times (1.74 \times 10^9 - 6.54 \times 10^8 \ln w)$$

where the units of E are nmol/m^2/day, w is wind speed (m/s), $[O_3]$ is surface ozone concentration (ppb), and $[I^-_{aq}]$ is aqueous iodide concentration (mol/dm^3). Sea surface temperature (SST, K) is used as the basis for estimating $[I^-_{aq}]$ (MacDonald et al.,2014):

$$[I^-_{aq}] = 1.46 \times 10^6 e^{\left(\frac{-9134}{SST}\right)}$$

A dependency on SST is consistent with measurements compiled by Chance et al. (2014). The range of $[I^-_{aq}]$ generated by CAM-Chem, with a mean 50 nmol/dm^3, agrees with the interquartile range of 28–140 nmol/dm^3 reported by Chance et al. (2014). However, Prados-Roman et al. (2015) note that the parameterization for $[I^-_{aq}]$ above yields lower concentrations than the SST^2 dependence of Chance et al. (2014), and that O_3 deposition rates are related to ocean biogeochemistry (Ganzeveld et al., 2009). Including these factors would enhance Ix

emissions, particularly in regions with elevated O_3 and high oceanic iodide concentrations. With these considerations in mind, Prados-Roman et al. (2015) conclude that Ix fluxes estimated from the parameterizations above should be regarded as lower limits.

Figure 2-1 shows the spatial distribution of annual-mean Ix emissions from CAM-Chem. The global annual average was estimated to be 1.9 Tg/yr, of which 95% derives from HOI.

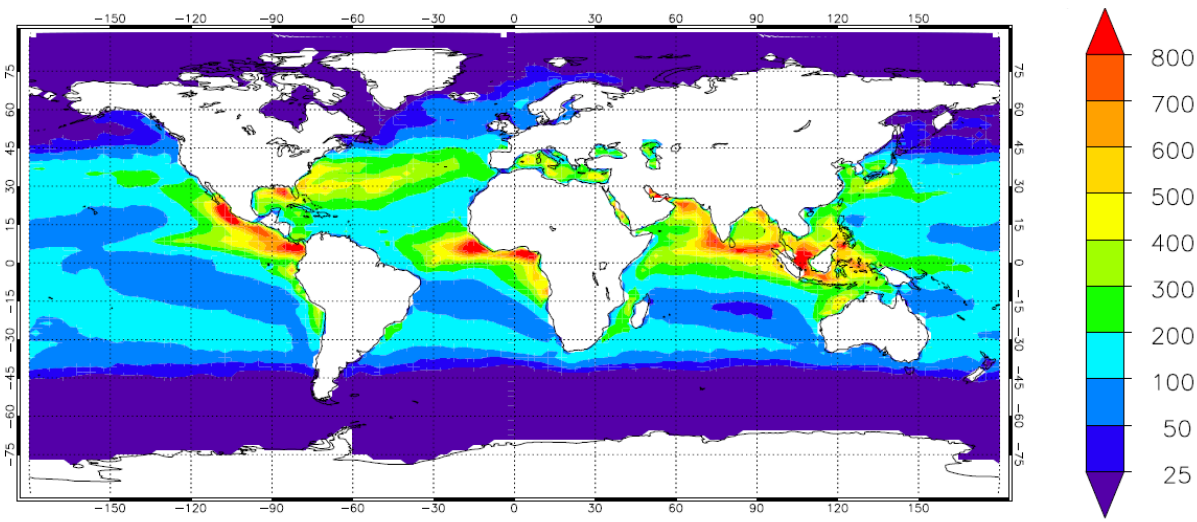

Figure 2-1. Annual mean Ix emission flux (nmol(Ix)/m^2/day) estimated by the CAM-Chem global chemistry-climate model, based on the parameterizations of Carpenter et al. (2013) and MacDonald et al. (2014). (From Figure 2 of Prados-Roman et al., 2015).

2.1 CAMx IMPLEMENTATION

We incorporated the CAM-Chem parameterizations for [I^-_{aq}], I_2 and HOI into an in-line emissions algorithm for CAMx. These parameterizations were first analyzed to ensure proper coding of the equations and to understand their sensitivity to three input parameters: layer 1 O_3 concentration, layer 1 wind speed, and surface temperature (equivalent to SST). Table 2-1 shows results from our sensitivity analysis assuming a constant 40 ppb ambient surface O_3 concentration in all cases.

A strong sensitivity to SST is noted for [I^-_{aq}], with almost a two order of magnitude change between 275 and 305 K. At conditions typical of the Gulf of Mexico (SST = 295 K or 72°F), [I^-_{aq}] concentrations are roughly 50 nmol/dm^3, which is consistent with the global/annual mean reported by Prados-Roman et al. (2015). Table 2-1 shows Ix fluxes for three wind speeds and four SST values. A similarly strong sensitivity to SST and wind speed is shown for Ix emissions. For a wind speed of 3 m/s (~7 MPH) and SST of 295 K (Table 2-1a), total emissions of 800 nmol(Ix)/m^2/day are very consistent with the annual mean shown for the Northeast Gulf region in Figure 2-1. Ix emissions increase by factors of 3-5 for a wind speed of 1 m/s (~2 MPH), but decrease by factors of 2-5 for a wind speed of 5 m/s (~11 MPH). HOI represents 91-99% of the total Ix emissions flux over all values shown in Table 2-1, again consistent with Prados-Roman et al. (2015).

Table 2-1(a). Aqueous iodide concentration [I^-_{aq}] and I_2, HOI and total Ix emission fluxes (Ix = HOI + 2×I_2) estimated using the parameterizations described by Prados-Roman et al. (2015) for surface ozone concentration of 40 ppb and wind speed of 3 m/s.

SST (K)	[I^-_{aq}] (nmol/dm^3)	I_2 Flux (nmol(Ix)/m^2/day)	HOI Flux (nmol(Ix)/m^2/day)	Ix Flux (nmol/m^2/day)	I_2 Fraction of Ix	HOI Fraction of Ix
275	5	0.7	65	66	2%	98%
285	18	3	334	341	2%	98%
295	52	14	774	801	4%	96%
305	143	52	1467	1571	7%	93%

Table 2-1(b). As in Table 2-1(a), but for wind speed of 1 m/s.

SST (K)	I_2 Flux (nmol(Ix)/m^2/day)	HOI Flux (nmol(Ix)/m^2/day)	Ix Flux (nmol/m^2/day)	I_2 Fraction of Ix	HOI Fraction of Ix
275	1	336	338	1%	99%
285	6	1253	1265	1%	99%
295	24	2752	2799	2%	98%
305	89	5117	5294	3%	97%

Table 2-1(c). As in Table 2-1(a), but for wind speed to 5 m/s.

SST (K)	I_2 Flux (nmol(Ix)/m^2/day)	HOI Flux (nmol(Ix)/m^2/day)	Ix Flux (nmol/m^2/day)	I_2 Fraction of Ix	HOI Fraction of Ix
275	0.5	11	12	8%	92%
285	2	150	155	3%	97%
295	9	378	397	5%	95%
305	35	737	807	9%	91%

As shown in Figure 2-1, total emissions range 300-800 nmol(Ix)/m^2/day in the northern Gulf of Mexico. In past TCEQ work addressing halogen chemistry, Yarwood et al. (2012 and 2014) applied a zero HOI flux and assumed a uniform I_2 emission flux of 1148 nmol(Ix)/m^2/day, representing a midpoint in the range of Ix estimates found in the literature. The new parameterizations using [O_3]=40 ppb, w=3 m/s and SST=295 K result in an HOI flux of 774 nmol(Ix)/m^2/day and an I_2 flux of 28 nmol(Ix)/m^2/day.

A new routine is called by the CAMx emissions injection algorithm at each model time step to calculate I_2 and HOI fluxes for each ocean grid cell according to fractional ocean coverage, surface layer ozone concentration, surface layer wind speed, and surface temperature. These emissions fluxes are added as new fields to the CAMx deposition output files so that they can be plotted and analyzed.

This modification, in combination with the condensed halogen chemistry mechanism described in Section 3 that removes reactions involving halomethane compounds, eliminates the need to run the SEASALT pre-processor to generate iodine emissions. Externally supplied emissions files should not include I_2 or HOI emissions to avoid double-counting. The in-line iodine emissions

routine requires that the optional ocean-land mask be included in the CAMx O3MAP input file to define over-ocean cells. These fields are identical to that used by the SEASALT pre-processor for consistency.

Figure 2-2 displays plots of daily total I_2 and HOI emissions over the Gulf of Mexico for June 18, 2006, from the offline SEASALT preprocessor and the new in-line calculation. Emissions are expressed in terms of Ix for comparability (Ix = HOI + 2×I_2). The in-line emissions are specific to the CAMx simulation (described in Section 4) and show spatial variations that contrast with the uniform emission rate assumed in SEASALT.

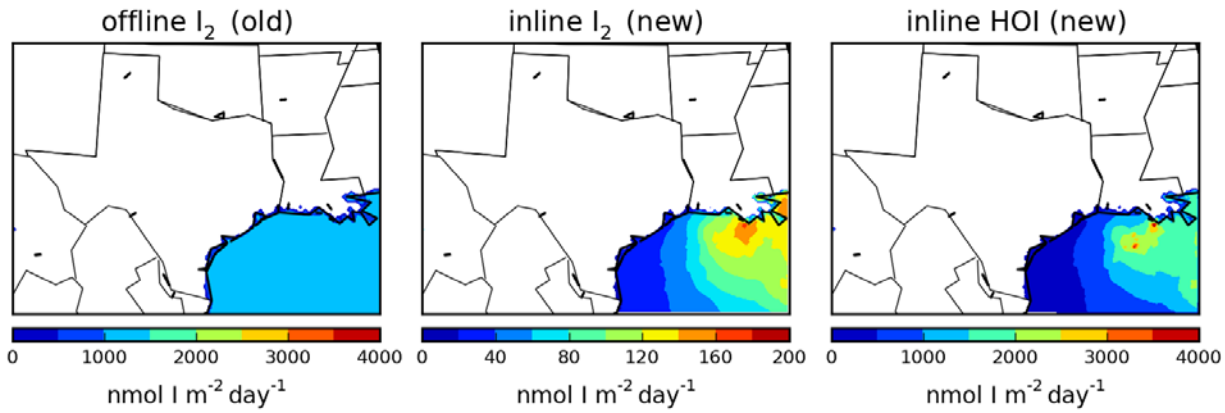

Figure 2-2. Estimated Ix emissions in the TCEQ 12 km modeling grid on June 18, 2006 in units of nmol(Ix)/m^2/day. The "offline" plot shows emissions generated by the SEASALT processor assuming uniform emissions at 1148 nmol(Ix)/m^2/day. The "in-line" plots show emissions generated within CAMx according to the equations of Prados-Roman et al. (2015). Note the difference in color scale for "in-line I_2".

3.0 IODINE MECHANISM CONDENSATION

The full iodine mechanism in CB6r2h includes 30 reactions (Yarwood et al., 2012). We investigate the roles of these reactions through a comprehensive sensitivity analysis. We identify a reduced set of reactions that are key to the dynamics of the full iodine mechanism, especially the extent and efficiency of O_3 depletion under environmental conditions typical of the marine boundary layer of the Gulf of Mexico. This compact iodine mechanism increases the efficiency of CAMx simulations of halogen-driven O_3 depletion.

3.1 Sensitivity Analysis of Iodine Reactions

We conducted sensitivity analysis of iodine reactions using the Decoupled Direct Method (DDM; Dunker, 1984) within a box model configuration of CAMx. The flexibility and efficiency of the box model and the DDM allow for a comprehensive sensitivity analysis of iodine chemistry across a spectrum of carefully designed modeling experiments.

3.1.1 Model Description

We configured CAMx to run as a box model to simulate photochemistry in the marine boundary layer over the Gulf of Mexico. The model simulated the full gas-phase chemistry using CB6r2 (216 reactions) along with iodine-only halogen chemistry from CB6r2h (30 reactions; Yarwood et al., 2014). Dry deposition was treated using the Wesley (1989) scheme. The model had a vertical depth of 150 m, representing the typical depth of marine boundary layer. The initial conditions, meteorological variables (assuming cloud-free conditions), and photolysis rates were extracted from a selected cell within the 12 km CAMx model domain (i = 120, j = 15, k = 1), where halogen-driven O_3 depletion was most active in our earlier CAMx simulations (Yarwood et al. 2014). The I_2 emission flux was set to 25 nmol m^2 hr^{-1}. Emissions of other iodine species were omitted for simplicity. To test the robustness of our findings to the variation of I_2 emissions, we extended our analysis to a spectrum of conditions, including 0.5, 1, 1.5, 2, 2.5, 5, 10, 15, 20 nmol m^2 hr^{-1} of I_2 emissions. The model was run for 24 hours, starting from local midnight on June 16, 2006.

3.1.2 Results and Discussion

We used CAMx DDM to calculate first-order, semi-normalized, local sensitivities (S_{ij}) of modeled concentrations (C_i) to a scaling factor (λ_j) applied to the rate constant for reaction j, i.e., $S_{ij} = \partial C_i / \partial \lambda_j$. The first-order response of O_3 to scaling the jth reaction rate constant by λ_j can be calculated with Equation (1), which represents a linear extrapolation:

$$\Delta C_i(\lambda_j) = S_{ij} \times \lambda_j \quad (1)$$

In addition to the sensitivities to individual iodine reactions, we also calculated the sensitivities to the scaling factor, denoted by λ_{I30}, of the group of all 30 iodine-involving reactions (I30), denoted by $S_{i,I30}$:

$$\Delta C_i(\lambda_1, \lambda_2, \lambda_3, \dots, \lambda_{30}) = S_{i,I30} \times \lambda_{I30} \quad (2)$$

When λ_j = 1 (j = 1, 2, 3, … 30) and λ_{I30} = 1:

$$S_{i,I30} = \Delta C(\lambda_1, \lambda_2, \lambda_3, \ldots, \lambda_{30}) = \sum_{j=1}^{30} \Delta C_i(\lambda_j) = \sum_{j=1}^{30} S_{ij} \qquad (3)$$

Equation (3) suggests that, in the first-order case, the sensitivity to a group of reactions equals the sum of sensitivities for individual reactions in the group. Indeed, we have confirmed that the sum of 30 individual sensitivities, S_{ij}, (j = 1, 2, 3, …, 30) agrees with the group sensitivity $S_{i,I30}$ to within 0.04%.

CAMx DDM has been used to estimate the impact of uncertain rate constants on modeled O_3 sensitivity to O_3 precursor emissions, by applying a scaling factor λ_j that reflect the range of uncertainty to a higher-order form of Equation (1) (Cohan et al., 2010). The semi-normalized sensitivities here are in essence equivalent to the dimensionless sensitivities calculated by some other authors for chemical sensitivity analysis, which were used to rank the importance of reactions (Pandis and Seinfeld, 1989) or to estimate the impact of uncertain rate constants (Dubey, 1997). We show in this study that the property illustrated by Equation (3), namely that semi-normalized, first-order sensitivities can be summed over individual reactions, can be also very useful in the context of developing a compact chemical mechanism.

Figure 3-1 shows O_3 sensitivities to individual reactions normalized to S_{I30}. Positive sensitivities are indicative of net O_3 depletion from the reaction (group), while negative sensitivities indicate the opposite effect. The reaction that has the largest O_3 depletion effect is IO + HO2 = HOI (+ O2), indicating that the IO + HO_2 catalytic cycle dominates O_3 depletion in the box model and that the reaction IO+HO_2 is the rate limiting reaction in the cycle (Figure 3-2). Similarly, OIO photolysis has the second largest sensitivity, indicating the secondary role of the IO + IO cycle, followed by the relatively smaller sensitivity to IO + NO2 = IONO2, a key step of the IO + NO_2 cycle. Such roles of the three catalytic cycles found in our box model are similar to the box modeling results during EASE-97 and ACE-2 campaigns over Northern and Eastern Atlantic Ocean (McFiggans et al. 2000).

Three reactions that counteract or limit O_3-depletion by iodine are OIO + OIO = IXOY, IO + IO = 0.4I + 0.4OIO + 0.6I2O2, and I2O2 + O3 = IXOY, all of which ultimately lead to the conversion of iodine radicals into I_XO_Y in the aerosol phase. The reaction OIO + OIO = IXOY is the least important of the three.

The negligible sensitivities of reactions involving MI_2, MIB, MIC, and CH_3I are expected because emissions of these species are omitted from our box model. These reactions are not considered for the compact iodine mechanism based upon the small contribution of these halo-methane species to the iodine radical budget in 3-D simulations (Yarwood et al., 2014).

Sensitivity analysis also revealed a number of reaction pairs with "symmetric" sensitivities, such as I + NO2 = INO2 and INO2 = I + NO2, that almost entirely cancel out each other's impact on O_3. These symmetric sensitivities reveal that scaling up (or down) the rate constant of either reaction in the pair by X% would have equal but opposite impact on O_3, but the fact that the sensitivity sum for the pair is almost zero does not necessarily indicate the reaction pair could

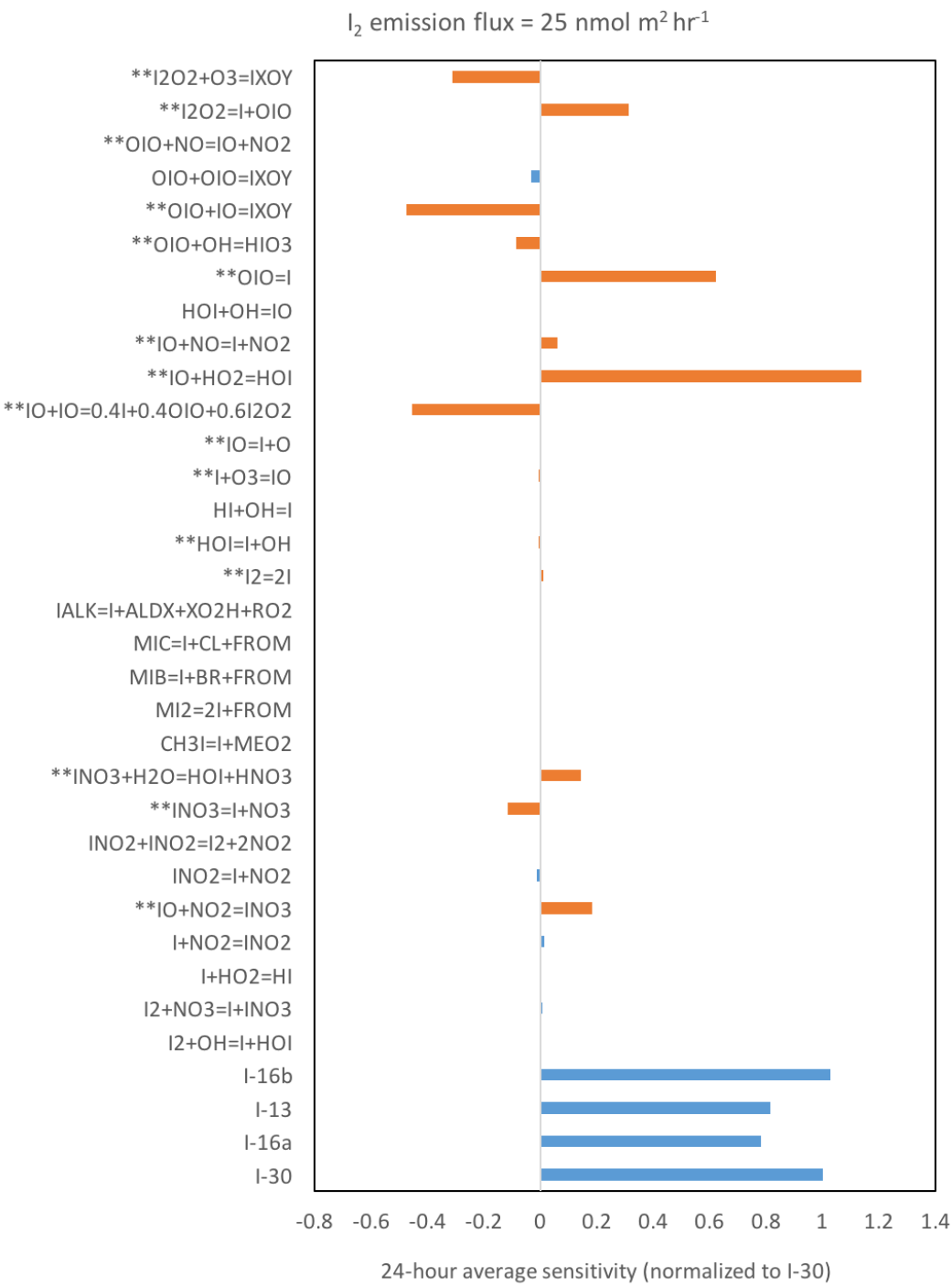

Figure 3-1. 24-hour average O_3 sensitivity to rate constants of individual (or groups of) reaction(s), with $E(I_2)$ = 25 nmol m^2 hr^{-1}. Reactions shown in orange and tagged with "" are those included in the 'I16b' compact iodine mechanism.**

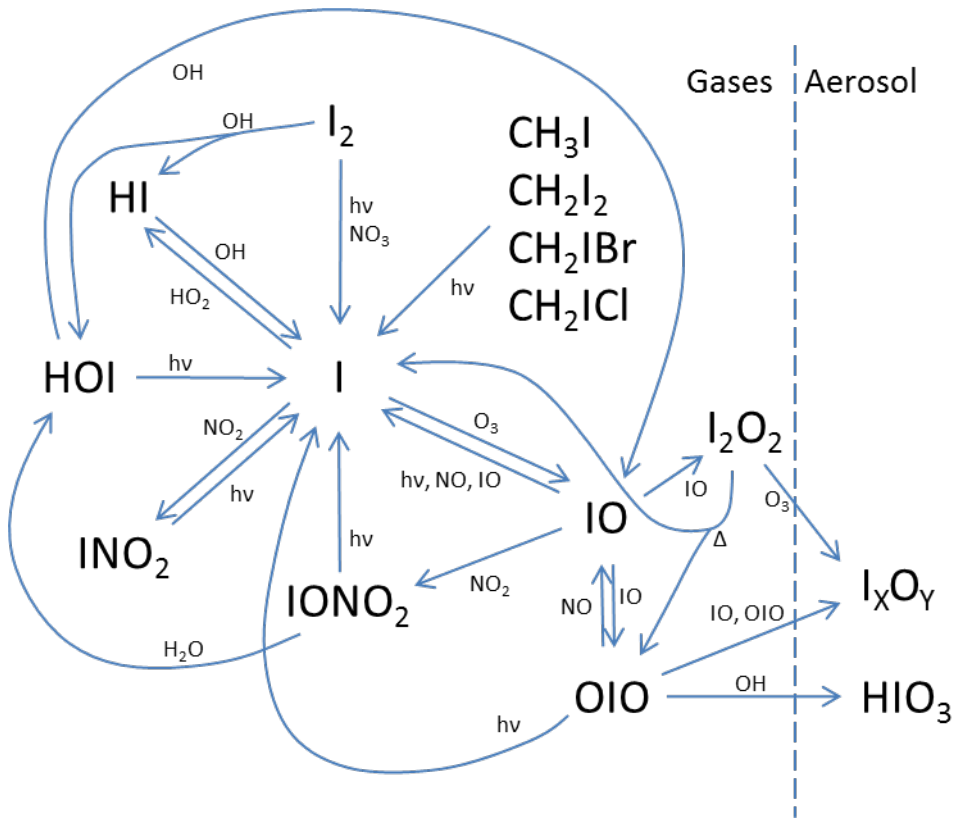

	IO + HO_2 cycle	*IO + IO cycle*	*IO + NO_2 cycle*
	$I + O_3 \rightarrow IO + O_2$	$(I + O_3 \rightarrow IO + O_2) \times 2$	$I + O_3 \rightarrow IO + O_2$
	$IO + HO_2 \rightarrow HOI + O_2$	$IO + IO \rightarrow I + OIO$	$IO + NO_2 \rightarrow IONO_2$
	$HOI + hv \rightarrow I + OH$	$OIO + hv \rightarrow I + O_2$	$IONO_2 + hv \rightarrow I + NO_3$
			$NO_3 + hv \rightarrow NO + O_2$
			$NO + O_3 \rightarrow NO_2 + O_2$
Net:	$O_3 + HO_2 \rightarrow OH + 2\ O_2$	$2\ O_3 \rightarrow 3\ O_2$	$2\ O_3 \rightarrow 3\ O_2$

Figure 3-2. Schematic of the full iodine chemistry mechanism (I-30) in CB6r2h.

be eliminated as a condensation strategy. Another reaction pair with symmetric sensitivities are the I_2O_2 removal reactions, namely I2O2 + O3 = IXOY and I2O2 = I + OIO, which could not be removed as a condensation strategy because they control the removal of reactive iodine.

The lack of O_3 sensitivity to some "essential" reactions is also notable. For example, without the reaction I + O3 = IO + O2 there can be no O_3 depletion by iodine. Lack of first-order sensitivity to the rate constant for this reaction indicates that its rate is more than fast enough in comparison to the rates of other reactions. However, O_3 depletion would cease if the rate constant for I + O3 was set to zero, indicating a non-linear relationship of O_3 to reducing the rate constant. This is an example that shows how the first-order local sensitivity calculated by DDM may not accurately describe the effects of some large rate constant perturbations.

The *local* sensitivities calculated by DDM may be restricted to (1) small perturbations in the rate constants for reactions that are strongly nonlinear, and (2) the particular chemical environment defined by emissions, meteorology, and initial and boundary conditions. The first restriction is not an issue for this work, as we are interested in the relative importance of individual reactions with their current rate constants, rather than the consequence of changing rate constants. However, in order to use the sensitivities to derive a compact mechanism, it is important to test the robustness of the sensitivities, and hence, the applicability of the mechanism, under different chemical environments, especially the possible variation of iodine enrichment in a 3-D modeling domain.

To understand how iodine chemistry behaves with different levels of iodine enrichment, we performed CAMx simulations and DDM sensitivity analyses for several I_2 emission fluxes (0.5, 1, 1.5, 2, 2.5, 5, 10, 15, 20 nmol m^2 hr^{-1}). Figure 3-3 (a) shows that depleted O_3 ($d[O_3] = [O_3] - [O_3]_{E(I_2)=0}$) appears to be a non-linear function of I_2 emission flux. Such non-linearity is confirmed by DDM sensitivity results. Figure 3-3 (b and c) show the sensitivities of O_3 and I_XO_Y to I_2 emission flux, respectively. I_XO_Y represents aerosol-phase iodine and its formation removes reactive iodine from the gas-phase. The absolute value of O_3 sensitivity, $|\partial[O_3]/\partial E(I_2)|$, decreases by a factor of 9 as I_2 emissions increase from 0.5 to 25 nmol m^2 hr^{-1}, while $\partial[I_XO_Y]/\partial E(I_2)$ increases by ~30%. Together, these two results suggest that the same amount of I_2 emission would cause much more O_3 depletion at lower than at higher I_2 enrichment, whereas iodine aerosol formation does not vary much with I_2 enrichment. This result is better illustrated in Figure 3-3 (d) by the chemical indicator ratio $\partial[O_3]/\partial[I_XO_Y]$, obtained here as the ratio of $\partial[O_3]/\partial E(I_2)$ and $\partial[I_XO_Y]/\partial E(I_2)$. Since the formation of I_XO_Y is indicative of the net loss of iodine available for O_3 destruction, $|\partial[O_3]/\partial[I_XO_Y]|$ quantifies *how many O_3 molecules are depleted per I_XO_Y molecule formed* and provides a measure for the efficiency of the catalytic iodine-driven O_3 depletion. $|\partial[O_3]/\partial[I_XO_Y]|$ decreases dramatically from ~3800 to ~155 as I_2 emission increases from 0.5 to 10 nmol m^2 hr^{-1}, and then plateaus as I_2 emission further increases. This characteristic of $|\partial[O_3]/\partial[I_XO_Y]|$provides direct evidence that the chemistry is different with different I_2 emissions, and underscores the need to examine the robustness of reaction sensitivity results in Figure 3-1 against I_2 emissions variation.

We calculated reaction rate constant sensitivities with I_2 emission fluxes at 10 and 1 nmol m^2 hr^{-1}, representing two conditions with likely different chemical dynamics, based on the results in Figure 3-3. Results are presented in Figure 3-4 and Figure 3-5, respectively. By a comparing Figure 3-1, Figure 3-4, and Figure 3-5, we find that the dominant reactions do not change as I_2 emissions change, despite the varying relative importance of individual reactions. At all I_2 emission levels, IO + HO2 = HOI is the largest contributor to O_3 depletion, followed by OIO photolysis and IO + NO2 = IONO2, suggesting the persistent simultaneous functioning of all three catalytic cycles regardless of how I_2 emission varies. At all emission levels, the dominating iodine sinks found in Figure 3-1 remain the same, with the IO + IO reaction being the largest sink. Comparing Figure 3-1 and Figure 3-5 also reveals that as iodine species are depleted, the chemistry becomes increasingly sensitive to the I-IO null cycle reactions, although O_3 depletion is still dominated by the overwhelmingly large contribution from IO + HO2 reaction.

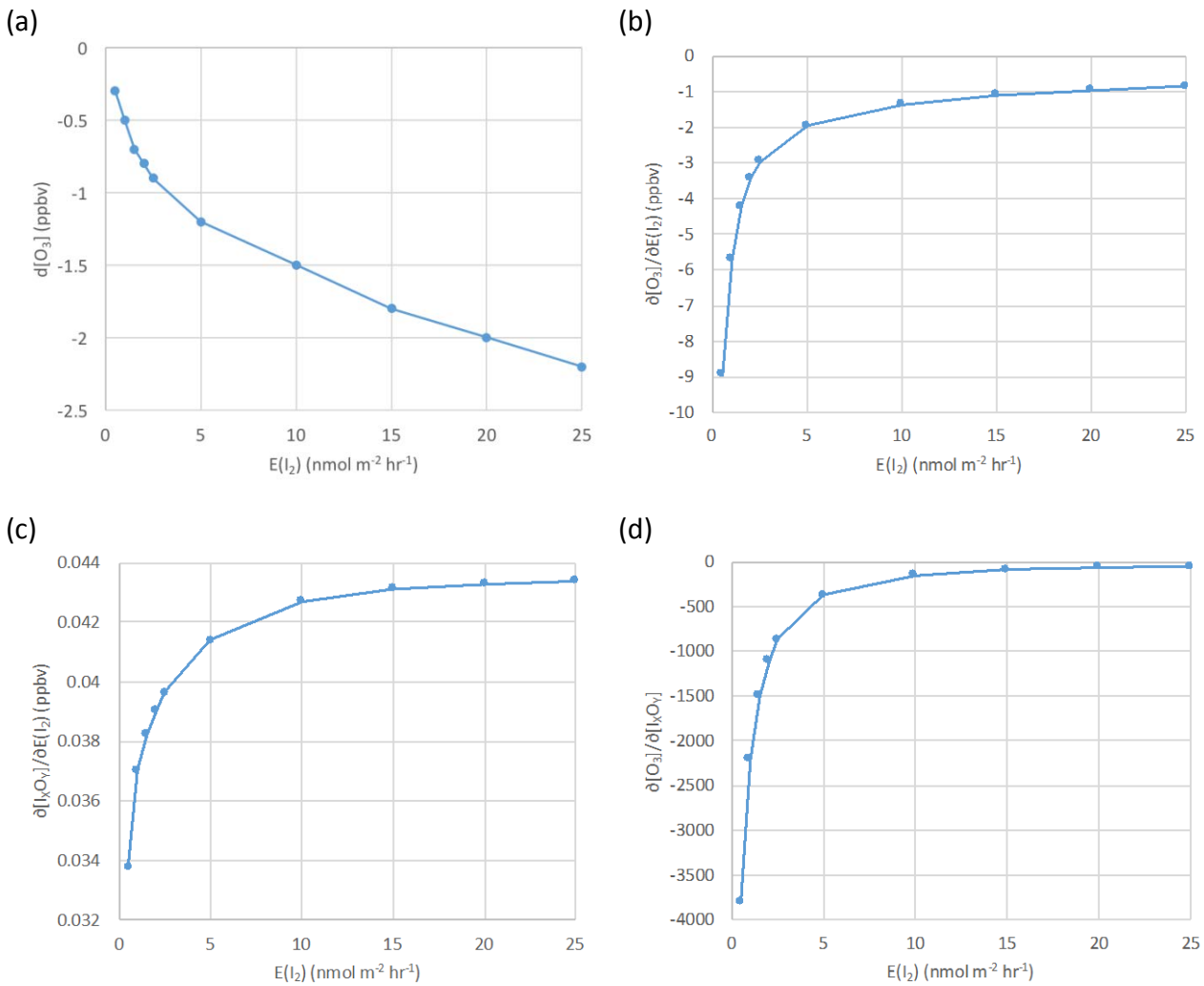

Figure 3-3. 24-hour average of (a) change in O_3 as a function of I_2 emissions, (b) O_3 sensitivity to I_2 emissions, (c) I_XO_Y sensitivity to I_2 emissions, and (d) sensitivity of O_3 to I_XO_Y ($\partial[O_3]/\partial[I_XO_Y]$), at different I_2 emission fluxes.

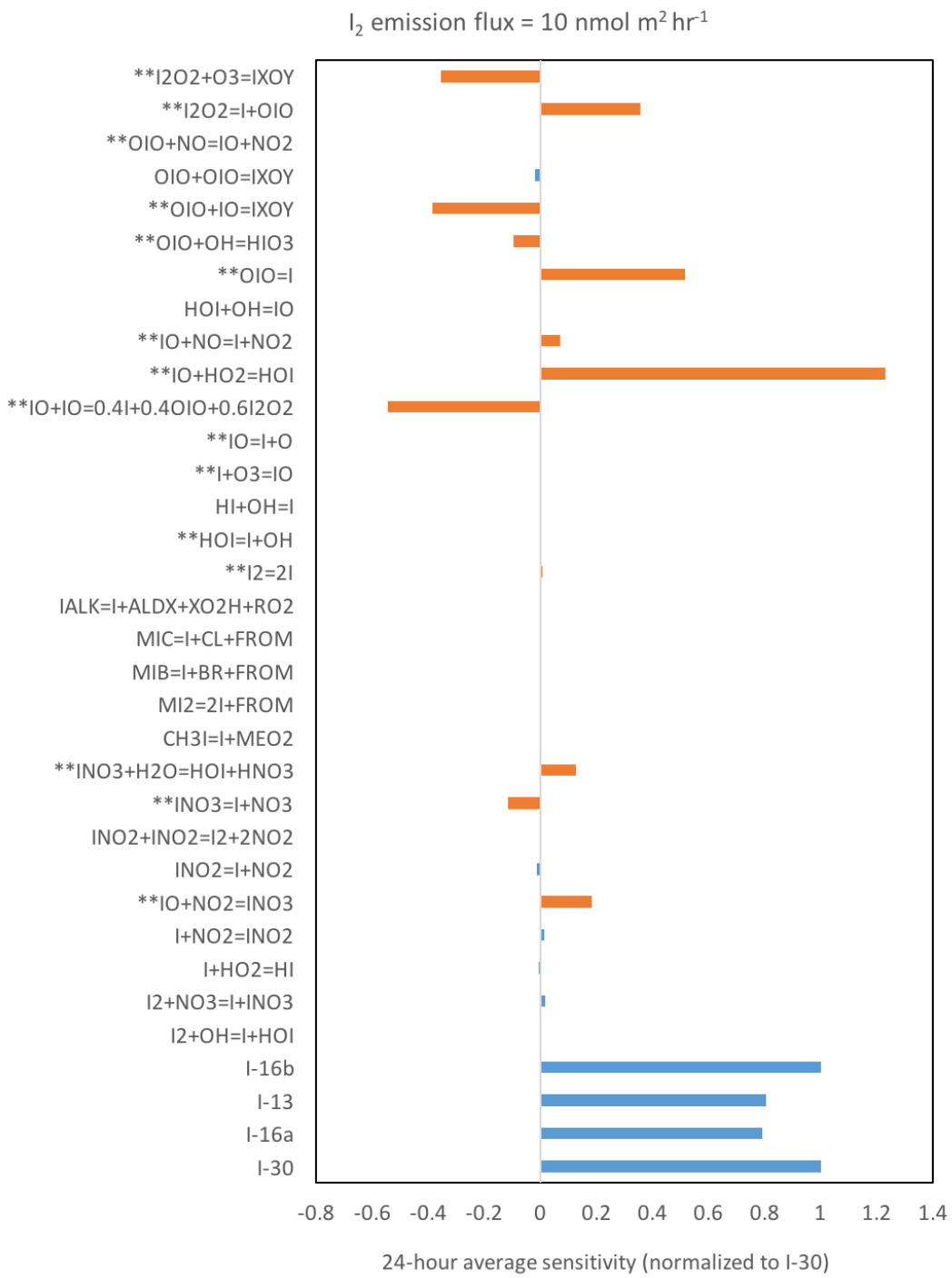

Figure 3-4. Same as Figure 3-1, but with $E(I_2)$ = 10 nmol m^2 hr^{-1}.

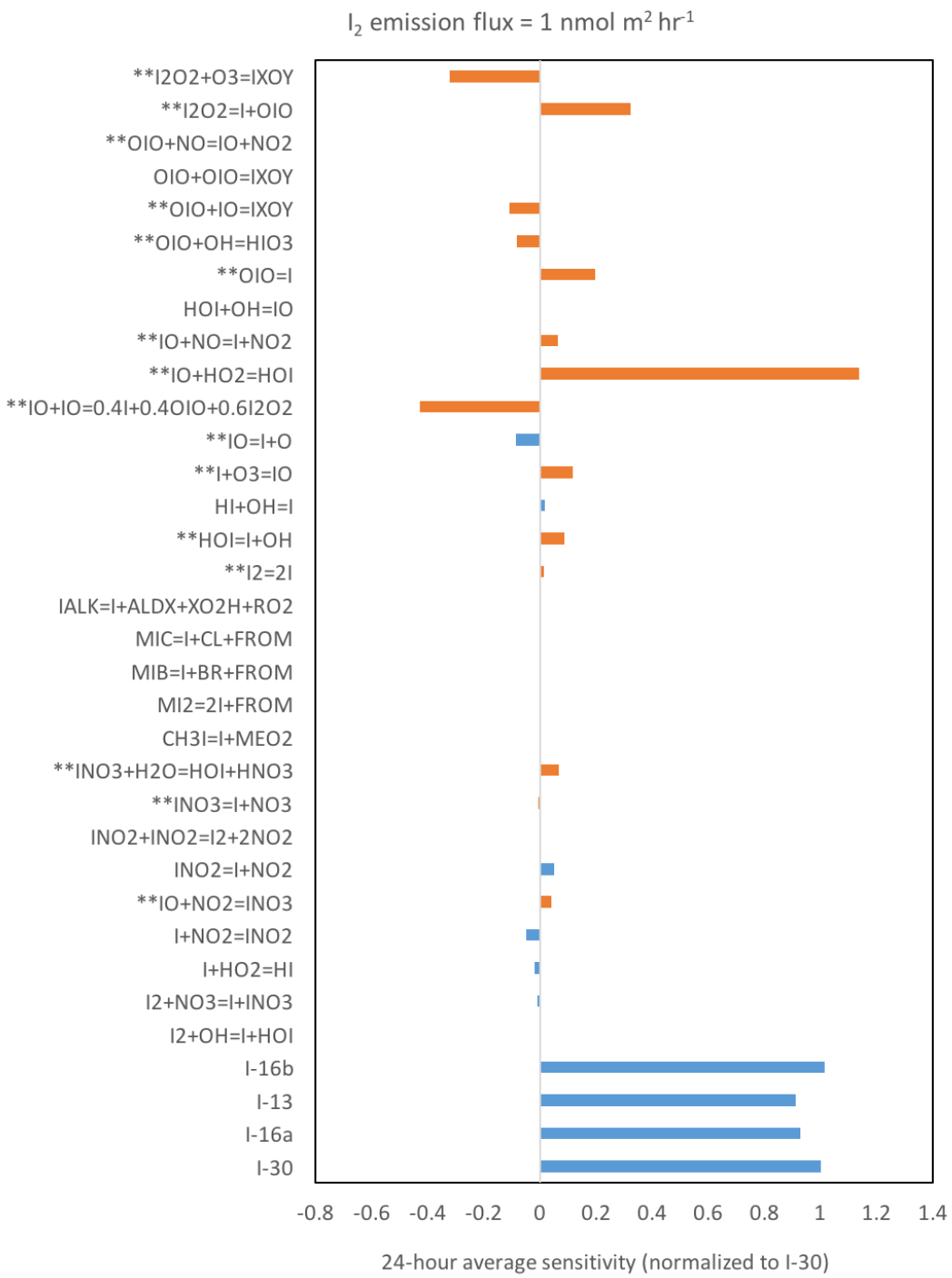

Figure 3-5. Same as Figure 3-1, but with $E(I_2)$ = 1 nmol m^2 hr^{-1}.

Overall, the results from our comprehensive CAMx DDM sensitivity analysis lead us to the following conclusions:

- The efficiency of O_3 depletion is highly dependent on iodine enrichment; therefore, accurately representing important iodine precursors (e.g., HOI) is critical for the fidelity of a 3-D model simulation of iodine chemistry.
- At all iodine enrichment levels tested (I_2 emission from 0.5 - 25 nmol m^2 hr^{-1}) O_3 depletion is consistently dominated by the IO + HO2 cycle, although two other catalytic cycles, i.e., IO + IO, and IO + NO2, are also depleting O_3.
- The extent of O_3 depletion by the IO + HO2 cycle is strongly affected by the availability of HO_2 radical.
- Reactions that convert gas phase iodine species into aerosols (represented by IXOY and HIO3) ultimately limit O_3 depletion by iodine. We consider these aerosol-forming reactions to be the least certain part of our iodine mechanism. This underscores the need for future studies to account for the model sensitivities to such chemical uncertainties in assessing iodine-driven O_3 depletion.

Our results show that there are a sub-group of reactions in the full iodine mechanism that are consistently the key drivers of chemistry across a spectrum of I_2 emissions. This finding provides the rationale for developing a compact mechanism that is suitable for a 3-D model with spatio-temporally varying I_2 emissions. In the next section, we select a subset of reactions that forms the compact iodine mechanism, based on the findings from our comprehensive sensitivity analysis.

3.2 Compact Iodine Mechanism

In light of the findings from the sensitivity analysis, we considered a subset of reactions that (1) have an aggregated sensitivity (ideally) equaling I-30 (the full iodine mechanism), and (2) include all the essential reactions needed by the three catalytic cycles (Figure 3-2). After some tests with the reaction sensitivities, 16 reactions tabulated in Table 3-1 (as highlighted in Figure 3-1, Figure 3-4, and Figure 3-5) were selected to form a compact mechanism referred to as "I-16b". The aggregated sensitivity with these reactions is 101% of the group sensitivity for I-30. The I-16b mechanism retains those reactions that constitute the three catalytic cycles, as well as the dominating iodine sinks. The 5 reactions involving iodine-containing halomethanes are all eliminated. The two reactions consisting of the null cycle of I + NO2 are also eliminated, considering their negligible impact on O_3 and other species. A few other reactions involving HI, OH, and NO_3 are also eliminated given their minor roles.

Two alternative subsets of reactions, I-16a and I-13 were also considered, as contrasting examples that illustrate the roles of key versus minor reactions. The difference of I-16a and I-13 from I-16b is the elimination of three key reactions for the IO + NO2 cycle: i.e., IO + NO2 = INO3, INO3 = I + NO3, INO3 + H2O = HOI + HNO3. I13 differs from I16a by eliminating three other reactions with small sensitivities: i.e., HI + OH = I, HOI + OH = IO, and OIO + OIO = IXOY. Figure 3-1, Figure 3-4, and Figure 3-5 show that the elimination of the former three reactions

within the IO + NO_2 cycle leads to 10% – 20% less aggregated sensitivity from I-16b, while I-16a and I-13 do not differ much with or without the three reactions with low sensitivities that are not involved in the catalytic cycles.

In the next chapter, we present results from CAMx 3-D simulations that compare the performance of I-16b against the full iodine and full halogen mechanisms.

Table 3-1. Lists of reactions included in the full iodine mechanism (I-30), and in I-16b, I-16a and I-13 subgroups.

Reactions (I30)	I-16b	I-16a	I-13
I2+OH=I+HOI			
I2+NO3=I+INO3			
I+HO2=HI			
I+NO2=INO2			
IO+NO2=INO3	√		
INO2=I+NO2			
INO2+INO2=I2+2NO2			
INO3=I+NO3	√		
INO3+H2O=HOI+HNO3	√		
CH3I=I+MEO2			
MI2=2I+FROM			
MIB=I+BR+FROM			
MIC=I+CL+FROM			
IALK=I+ALDX+XO2H+RO2			
I2=2I	√	√	√
HOI=I+OH	√	√	√
HI+OH=I		√	
I+O3=IO	√	√	√
IO=I+O	√	√	√
IO+IO=0.4I+0.4OIO+0.6I2O2	√	√	√
IO+HO2=HOI	√	√	√
IO+NO=I+NO2	√	√	√
HOI+OH=IO		√	
OIO=I	√	√	√
OIO+OH=HIO3	√	√	√
OIO+IO=IXOY	√	√	√
OIO+OIO=IXOY		√	
OIO+NO=IO+NO2	√	√	√
I2O2=I+OIO	√	√	√
I2O2+O3=IXOY	√	√	√

4.0 TESTING AND EVALUATION

We tested the condensed halogen chemical mechanism described in Section 3 against non-halogen (CBr2) and original halogen (CBr2h) mechanisms using the TCEQ's "Rider 8" CAMx model of June 2006. This is the same dataset used by Yarwood et al. (2012, 2014) in prior halogen chemistry projects. All of the CAMx input data were obtained from the TCEQ with the exception of the oceanic halogen emissions and halomethane boundary conditions.

4.1 CAMx Tests

The TCEQ developed the CAMx "Rider 8" model for use by areas in Texas that are close to the National Ambient Air Quality Standard (NAAQS) for ozone but not designated as nonattainment areas. CAMx input data files were downloaded from: http://www.tceq.texas.gov/airquality/airmod/rider8/rider8Modeling. In summary, meteorological input data were developed using the Weather Research Forecasting (WRF) model and WRFCAMx interface; anthropogenic emissions were based on TCEQ data within Texas and data from EPA outside Texas; biogenic emissions were developed using MEGAN; and boundary conditions for the outer 36 km grid were extracted from a GEOS-Chem global model simulation of 2006.

The Rider 8 nested modeling grids are shown in Figure 1-1. The layer structure is defined in Figure 4-1 with 28 layers from the surface to 15 km and a surface layer depth of 34 m. The outer 36 km grid covers the continental US (CONUS) and is the same grid that EPA and many States use for regional air quality modeling. The nested 12 km grid covers Texas and a substantial area that would typically be upwind of Texas during an ozone episode including adjacent States and the western Gulf of Mexico. The nested 4 km grid covers the Houston and Dallas ozone nonattainment areas and all of the near nonattainment areas in eastern Texas. CAMx 2-way grid nesting is used to model all grids simultaneously so that pollution transport between grids is modeled without the need for boundary conditions for the nested grids.

Three CAMx runs were conducted:

- CB6r2h (Base) with 88 reactions and 33 species involving I, Br, and Cl
- I-30 with all previous 30 reactions and 16 species involving I
- I-16b with 16 reactions and 9 species involving I.

All tests used CAMx version 6.2 with the addition of in-line Ix emissions described in Section 2 in lieu of the uniform I_2 estimate set by Yarwood et al. (2012, 2014). Emissions of organic I (for I-30 and CB6r2h cases), and emissions of Br and Cl compounds (for the CB6r2h case), were derived using the SEASALT preprocessor as described by Yarwood et al. (2014). All tests were run for a three day period (00 CST June 16 through 00 CST June 18) employing only the 36 and 12 km grids. In all cases, initial conditions at 00 CST June 16 were taken from CAMx "restart" files from prior modeling conducted by Yarwood et al. (2014) using the full CB6r2h mechanism. Boundary conditions for all CAMx species were taken from files developed by Yarwood et al. (2014).

Vertical Layer Structure

Corresponding WRF Layer	Layer Top (m AGL)	CAMx Layer	Layer Center (m AGL)	Thickness (m)
38	15179.1	28	13637.9	3082.5
36	12096.6	27	10631.6	2930.0
32	9166.6	26	8063.8	2205.7
29	6960.9	25	6398.4	1125.0
27	5835.9	24	5367.0	937.9
25	4898.0	23	4502.2	791.6
23	4106.4	22	3739.9	733.0
21	3373.5	21	3199.9	347.2
20	3026.3	20	2858.3	335.9
19	2690.4	19	2528.3	324.3
18	2366.1	18	2234.7	262.8
17	2103.3	17	1975.2	256.2
16	1847.2	16	1722.2	249.9
15	1597.3	15	1475.3	243.9
14	1353.4	14	1281.6	143.6
13	1209.8	13	1139.0	141.6
12	1068.2	12	998.3	139.7
11	928.5	11	859.5	137.8
10	790.6	10	745.2	90.9
9	699.7	9	654.7	90.1
8	609.7	8	565.0	89.3
7	520.3	7	476.1	88.5
6	431.8	6	387.9	87.8
5	344.0	5	300.5	87.1
4	256.9	4	213.8	86.3
3	170.6	3	127.8	85.6
2	85.0	2	59.4	51.0
1	33.9	1	17.0	33.9

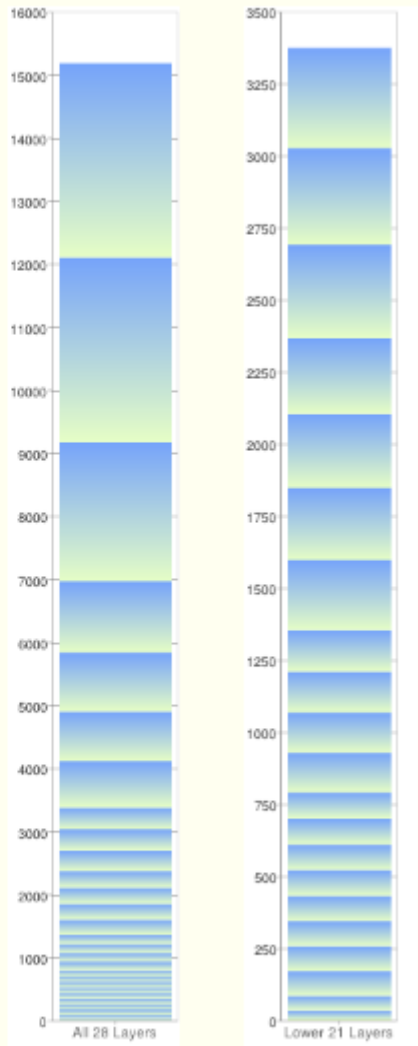

AGL - Above Ground Level.

Figure 4-1. CAMx vertical layer structure for the Rider 8 model of June 2006. TCEQ figure from http://www.tceq.texas.gov/airquality/airmod/rider8/modeling/domain.

4.1.1 Comparison of Ozone Impacts from Halogen Mechanisms

Figure 4-2 displays changes to simulated maximum daily 8-hour (MDA8) ozone on June 18, 2006 from the three halogen mechanisms (CB6r2h, I-30, and I-16b). The top panels show MDA8 ozone decrements relative to a no-halogen case (i.e., standard CB6r2), while the bottom panels show decrements relative to the full halogen case (i.e., CB6r2h). Figure 4-3 shows time series of ozone reductions relative to the non-halogen case at four coastal sites along the Gulf of Mexico.

As shown in both figures, iodine is responsible for most of the ozone depletion. The full halogen mechanism results in peak MDA8 ozone decrements of more than 7 ppb, while the I-30 and I-16B cases indicate decrements of over 5 ppb. Ozone depletion with I-16b is very similar to the I-30 case, as shown in the very similar difference patterns among the bottom panels of Figure 4-2 and Figure 4-3.

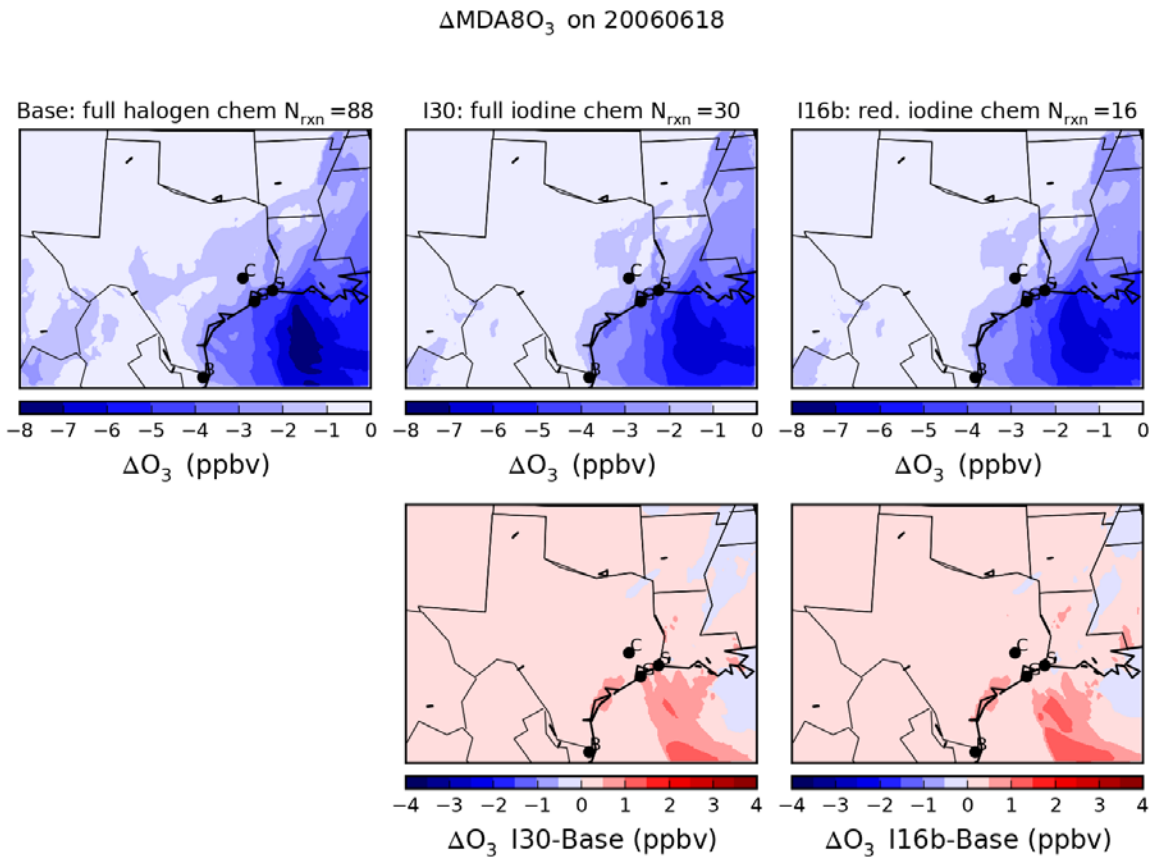

Figure 4-2. Changes in simulated MDA8 ozone on June 18, 2006 from three halogen mechanisms: CB6r2h (top left), I-30 (middle), and I-16b (right). Top panels show MDA8 ozone decrements relative to a no-halogen case using the standard CB6r2 mechanism, while the bottom panels show decrements resulting from I-30 and I-16b relative to the full halogen case (CB6r2h).

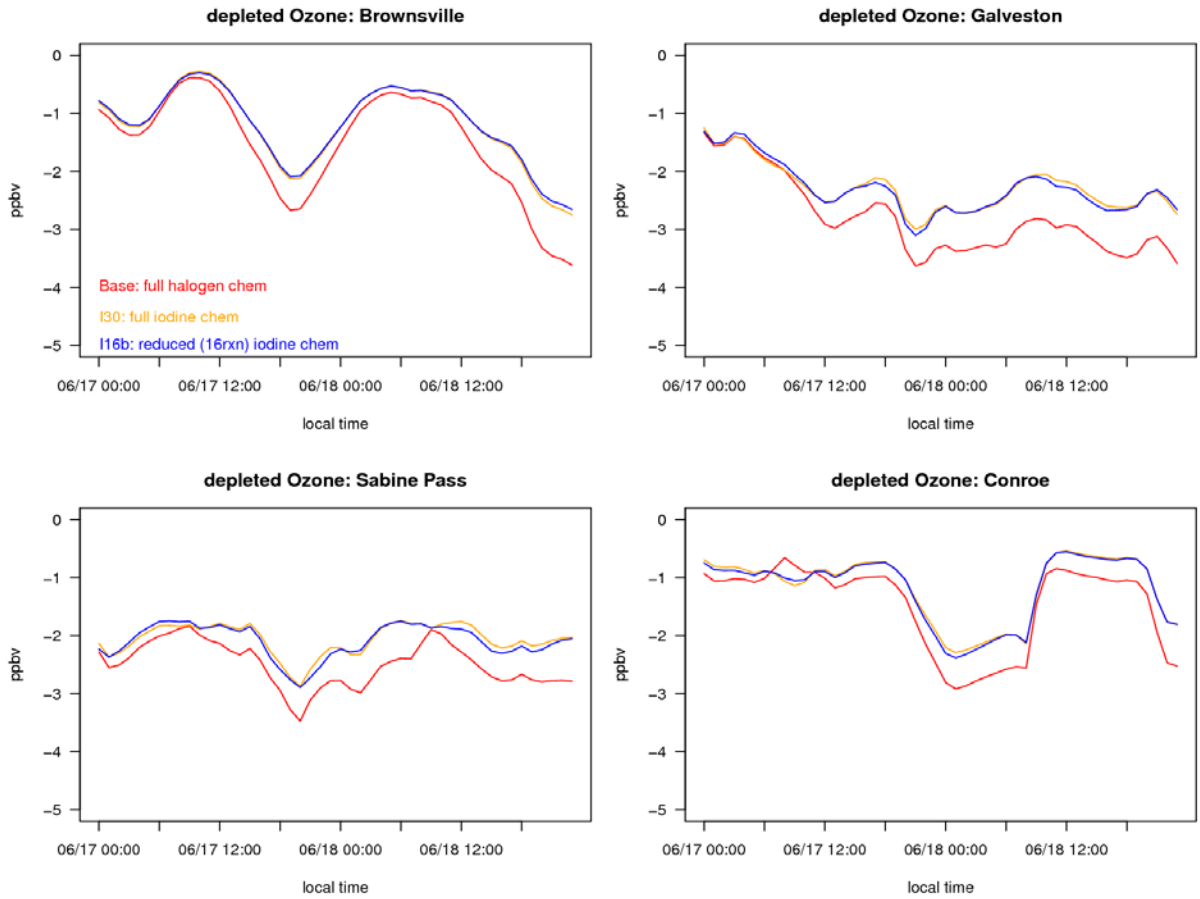

Figure 4-3. Time series at four coastal Gulf sites of hourly ozone reduction over June 17-18, 2006 from three halogen mechanisms: CB6r2h (red), I-30 (orange), and I-16b (blue). Ozone decrements are relative to a no-halogen case using the standard CB6r2 mechanism.

4.1.2 CAMx Speed Performance

Table 4-1 displays the absolute and relative run times for the three-day test period using non-halogen chemistry (CB6r2) and the CB6r2h and I-16b versions of halogen chemistry. While I-16b is faster than CB6r2h, it remains disproportionately slow relative to the non-halogen case because of stiff reactions involving I, IO and OIO species. A custom solver was developed to specifically address these reactions, resulting in some speed improvement. Additionally, the rate constant sensitivity results from Section 3 have allowed us to develop a strategy to update OSAT/APCA for ozone depletion by iodine and to account for impacts to nitrate.

Table 4-1. CAMx run times to simulate three days using three different chemical mechanisms on the 2006 TCEQ Rider 8 36/12 km grid system.

Mechanism	Time (min)	Percent of CB6
CB6r2h	52	226%
I-16b	39	170%
I-16b + Solver Update	36	156%
CB6r2	23	100%

4.2 CAMx Code Delivery

In April 2016, Ramboll Environ submitted an interim set of CAMx source code to TCEQ:

- CAMx v6.20 with condensed "I-16b" halogen chemistry and specialized solver
- I-16b replaces CB6r2h as Mechanism 3
- Includes in-line Ix emissions, written to deposition output files
- Does not include OSAT/APCA update
- Does not include model speed enhancements implemented by Ramboll Environ in 2015 for TCEQ (Emery et al., 2015) and publicly released as v6.30 in 2016

In May 2016, Ramboll Environ submitted a final set of CAMx source code to TCEQ:

- CAMx v6.31 with condensed "I-16b" halogen chemistry and specialized solver;
- I-16b added as Mechanism 1; CB6r2h remains as Mechanism 3
- Includes in-line Ix emissions (can be used with either I-16b or CB6r2h), written to deposition output files
- Includes OSAT/APCA update for ozone depletion by Ix and impacts to nitrate
- Merged with v6.30 to include 2015 model speed enhancements

4.3 Running CAMx with Condensed Halogen Chemistry

This section provides basic user instructions on using CAMx with the new halogen chemistry and in-line Ix emissions routine.

- Compile CAMx as you normally would.
- Add a new namelist flag "`Inline_Ix_Emissions`" to the CAMx namelist control file, set it to "`.TRUE.`" This eliminates the need for I_2 emissions in your input gridded emissions files. In-line estimates of I_2 and HOI emissions are output to the deposition output files for further analysis.
- If this flag is set to TRUE, you must supply your standard emissions without halogen estimates, otherwise CAMx will stop with an error.
- If this flag is set to FALSE, you may continue to use externally-derived halogen emissions from the SEASALT pre-processor.

- Add a "land/ocean" mask field to the O3MAP input file. This is described in the CAMx v6.30 User's Guide, Section 3.3. That section is replicated below (see Figure 4-4). The land/water mask is identical to the fields that are developed for the SEASALT pre-processor. It can simply be added "as-is" to your daily O3MAP files for each grid in your simulation.
- Continue to use your initial/boundary condition files that include halogens "as-is". Initial/boundary conditions for halogens may be developed using the updated GEOS-Chem model with new halogen chemistry (Work Order FY16-16).

4.3.1 Ozone Column File

This file defines the intervals of total atmospheric ozone column to be used by TUV, as well as its spatial and temporal distributions for a specific CAMx domain and episode. This parameter is essential for photochemical simulations as it determines the spatial and temporal variation of photolysis rates. Therefore, this file must be supplied if chemistry is invoked. Additionally, the ozone column file may also provide an optional field defining a land/ocean mask.

There are two mandatory and one optional header records in the ozone column file. The first record contains an arbitrary file label. The second record defines the intervals for 5 ozone column values for the domain and temporal period to be simulated. These intervals must exactly match those defined in preparing the photolysis rates file, so the ozone column file is also read by the TUV preprocessor to define the photolysis rates lookup table (Section 3.2).

If the optional land/ocean mask is included, then a third header record must be added to inform CAMx that this field is to be read. The time-invariant land/ocean mask is simply a map of 0 (land and fresh water bodies) and >0 (ocean) that must be located directly under its header record. A value must be supplied for each cell of the master grid and optionally any nested grids.

Gridded fields of time-varying ozone column follow the header records and optional land/ocean mask data. The gridded fields are maps of the respective "codes" for each interval, as defined in the header. For example, 5 ozone column intervals are specified in TUV and in the ozone column header record, so the map must consist of a distribution of integers ranging from 1 to 5. Ozone column is supplied for the master grid only; CAMx internally assigns master cell values to all nested grids cells. Multiple maps of these codes may be provided for arbitrary time intervals that span the entire simulation period.

The ozone column file is a readable text format and it has the following structure:

```
text                                (A)
ozname,(ozncl(n),n=1,nozn)          (A10,5F10.0)
loname,igrd,nx,ny                   (A10,3I10)        -- Optional
Loop from j = ny grid rows to 1                       -- Optional
   (jocn(i,j),i=1,nx)               (999I1)           -- Optional
loname,igrd,nx,ny                   (A10,3I10)        -- Optional
ozname,idt1,tim1,idt2,tim2          (A10,I10,F10.0,I10,F10.0)
Loop from j = ny master grid rows to 1
   (jozn(i,j),i=1,nx)               (9999I1)
```

where the variables in the ozone column file have the following definitions:

`text`	Text identifying file and any messages
`ozname`	Text string “OZONE COL”
`ozncl`	Ozone column (Dobson units) for each of *nozn* ozone values
`loname`	Text string “OCEAN”
`igrd`	Grid index (1 = master grid, 2+=nested grid, 0 = end of data)
`nx`	Number of grid columns for this grid index
`ny`	Number of grid rows for this grid index
`jocn`	Grid *igrd,* row *j* land/ocean codes for *nx* grid columns
`idt1`	Beginning date (YYJJJ) of time span
`tim1`	Beginning hour (HHMM) of time span
`idt2`	Ending date of time span
`tim2`	Ending hour of time span
`jozn`	Master grid row *j* ozone column codes for *nx* master grid columns

An example of a small ozone column file is given in Figure 4-4.

```
Sample ozone column file with optional land ocean mask
OZONE COL      0.285     0.315     0.345     0.375     0.405
OCEAN              1        64        10
0000000000000000000011111111100000000000000000000000000000000000
0000000000000000000000000001111111110000000000000000000000000000
0000000000000000000000000011111111111110000000000000000000000000
0000000000000000000000000001111111111110000000000000000000000000
0000000000000000000000011111111111111110000000000000000000000000
0000000000000000000000011111111111111111100000000000000000000000
0000000000000000000000011111111111111111110000000000000000000000
0000000000000000000000111111100000000011111111100000000000000000
0000000000000000000001111111110000000001111111110000000000000000
0000000000000000000011111111100000000000111111111000000000000000
OCEAN              0         0         0
OZONE COL      05213      0.00     05213   2400.00
3333333333333333333333333333333333333333333333333333333333333333
3333333333333333333333333333333333333333333333333333333333333333
2222222222222333333333333333333333333333333333333333333333333333
2222222222222222333333333333333333333333333333333333333333333333
2222222222222222333333333333333333333333333333333333333333333333
2222222222222222333333333333333333333333333333333333333333333333
2222222222222222333333333333333333333333333333333333333333333333
2222222222222222333333333333333333333333333333333333333333333333
2222222222222222333333333333333333333333333333333333333333333333
2222222222222222222222233333333333333333333333333333333333333333
```

Figure 4-4. Example structure of a single-grid ozone column input file showing panels for the optional time-invariant land-ocean mask and time-varying ozone column field.

5.0 CONCLUSION

Ramboll Environ improved both speed and accuracy in modeling ozone transported into Texas from the Gulf of Mexico by: 1) implementing a condensed halogen mechanism; and 2) implementing a reactive iodine (Ix) emissions algorithm within CAMx. The reason for implementing Ix emissions within CAMx (referred to as "in-line") is that the Ix emissions depend upon surface layer ozone concentration, wind speed and sea surface temperature (SST). CAMx outputs the spatially and temporally varying Ix emissions for diagnostic evaluation and reporting purposes. These updates are implemented in CAMx version 6.31.

Conclusions drawn from this work are listed below:

- According to the approach of Prados-Raman et al. (2015), oceanic iodide concentrations exhibit a strong exponential sensitivity to SST, resulting in a similarly strong Ix emissions sensitivity to SST and wind speed and a linear Ix emissions response to ambient ozone concentrations.
- For conditions typical of the Gulf of Mexico, HOI contributes 91-99% of the total Ix emissions flux with I_2 contributing the remainder.
- The new in-line algorithm results in Ix emission fluxes that range above and below the previous assumption of uniform I_2 emissions (Yarwood et al., 2014) that represented a midpoint in the range of Ix estimates found in the literature.
- DDM rate constant sensitivity analysis in CAMx proved to be a powerful method for analyzing the roles of individual halogen reactions and then developing a condensed halogen mechanism.
- Using insights gained from the DDM rate constant sensitivity analysis we updated the CAMx ozone source apportionment methods (OSAT and APCA) to account for ozone depletion by iodine and impacts to nitrate.
- We showed that the efficiency of ozone depletion by iodine is highly dependent on the amount of iodine enrichment; therefore, accurately representing important iodine precursors (e.g., HOI) is critical for the fidelity of simulating ozone depletion by iodine.
- We identified a sub-group of iodine-related reactions that are consistently the key drivers of ozone depletion across a range of Ix emission. Using this information we developed a compact 16-reaction mechanism with 9 inorganic iodine species ("I-16b").
- The compact I-16b mechanism retains reactions that constitute the three important catalytic cycles of ozone destruction by iodine, as well as the dominant iodine removal reactions (sinks).
- Ozone sensitivity to Ix emissions with the I-16b mechanism is almost 100% of the sensitivity with the 30 iodine reactions present in CB6r2h.
- In 3-day CAMx test runs based on the TCEQ Rider 8 modeling dataset for June 2006, the full halogen and condensed I-16b mechanisms produced similar peak MDA8 ozone decrements of 5-7 ppb over the Gulf of Mexico.

- CAMx run times for the 3-day test were reduced by 31% using I-16b relative to the full halogen mechanism, but remained 56% longer than the CB6r2 mechanism without halogen chemistry.

6.0 REFERENCES

Alicke, B., K. Hebestreit, J. Stutz, U. Platt. 1999. Iodine oxide in the marine boundary layer. *Nature*, 397, 572–573.

Carpenter, L.J. 2003. Iodine in the marine boundary layer. *Chemical Reviews*, 103, 4953-4962.

Carpenter, L.J., S.M. MacDonald, M.D. Shaw, R. Kumar, R.W. Saunders, R. Parthipan, J. Wilson, J.M.C. Plane. 2013. Atmospheric iodine levels influenced by sea surface emissions of inorganic iodine. *Nature Geoscience,* 6, no. 2: 108-111.

Chameides, W.L., and D.D. Davis. 1980. Iodine: Its Possible Role in Tropospheric Photochemistry. *J. Geophys. Res.*, 85, 7383–7398, doi:10.1029/JC085iC12p07383.

Chance, R., A.R. Baker, L. Carpenter, T.D. Jickells. 2014. The distribution of iodide at the sea surface. *Environmental Science: Processes & Impacts*, 16, 1841–1859, doi:10.1039/C4EM00139G.

Cohan, D.S., B. Koo, G. Yarwood. 2010. Influence of uncertain reaction rates on ozone sensitivity to emissions. *Atmos. Environ.*, 44, 3101-3109.

Dubey, M. K., G.P. Smith, W.S. Hartley, D.E. Kinnison, P.S. Connell. 1997. Rate parameter uncertainty effects in assessing stratospheric ozone depletion by supersonic aviation. *Geophys. Res. Lett*., 24, 2737-2740.

Dunker, A.M. 1984. The decoupled direct method for calculating sensitivity coefficients in chemical kinetics. *J. Chem. Phys*., 81, 2385-2393.

Emery, C., G. Wilson, D.J. Rasumussen, G. Yarwood. 2015. CAMx Speed Improvements. Final Report for Work Order No. 582-15-50417-FY15-35.

Federal Register. 2015. National Ambient Air Quality Standards for Ozone; A Rule by the Environmental Protection Agency on 10/26/2015. https://www.federalregister.gov/articles/2015/10/26/2015-26594/national-ambient-air-quality-standards-for-ozone.

Garland, J. A., and H. Curtis. 1981. Emission of iodine from the sea surface in the presence of ozone. *Journal of Geophysical Research: Oceans* (1978–2012), 86, no. C4: 3183-3186.

Ganzeveld, L., D. Helmig, C.W. Fairall, J. Hare, A. Pozzer. 2009. Atmosphere-ocean ozone exchange: A global modeling study of biogeochemical, atmospheric, and waterside turbulence dependencies. *Global Biogeochem. Cy.*, 23, GB4021, doi:10.1029/2008GB003301.

Harvard. 2015. GEOS-Chem web site and documentation: http://acmg.seas.harvard.edu/geos/.

Lamarque, J.F., L.K. Emmons, P.G. Hess, D.E. Kinnison, S. Tilmes, F. Vitt, C.L. Heald, E.A. Holland, P.H. Lauritzen, J. Neu, J.J. Orlando, P.J. Rasch, G.K. Tyndall. 2012. CAM-chem: description and evaluation of interactive atmospheric chemistry in the Community Earth System Model. *Geosci. Model Dev.*, 5, 369–411, doi:10.5194/gmd-5-369-2012.

MacDonald, S.M., J.C. Gómez Martín, R. Chance, S. Warriner, A. Saiz-Lopez, L.J. Carpenter, J.M.C. Plane. 2014. A laboratory characterisation of inorganic iodine emissions from the sea surface: dependence on oceanic variables and parameterization for global modelling. *Atmos. Chem. Phys.*, 14, 5841–5852, doi:10.5194/acp-14-5841-2014.

Mahajan, A.S., H. Oetjen, A. Saiz-Lopez, J.D. Lee, G.B. McFiggans, J.M.C. Plane. 2009. Reactive iodine species in a semi-polluted environment. *Geophys. Res. Lett.*, 36, L16803, doi:10.1029/2009GL038018.

Mahajan, A.S., J.M.C. Plane, H. Oetjen, L. Mendes, R.W. Saunders, A. Saiz-Lopez, C.E. Jones, L.J. Carpenter, G.B. McFiggans. 2010. Measurement and modelling of tropospheric reactive halogen species over the tropical Atlantic Ocean. *Atmos. Chem. Phys.*, 10, 4611-4624, 2010 doi:10.5194/acp-10-4611-2010.

McFiggans, G., J.M.C. Plane, B.J. Allan, L.J. Carpenter, H. Coe, C. O'Dowd. 2000. A modeling study of iodine chemistry in the marine boundary layer. *J. Geophys. Res.*, 105(D11), 14371–14385.

Pandis, S.N., and J.H. Seinfeld. 1989. Sensitivity analysis of a chemical mechanism for aqueous-phase atmospheric chemistry. *J. Geophys. Res.*, 94, 1105-1126.

Prados-Roman, C., C.A. Cuevas, R.P. Fernandez, D.E. Kinnison, J.F. Lamarque, A. Saiz-Lopez. 2015. A negative feedback between anthropogenic ozone pollution and enhanced ocean emissions of iodine. *Atmospheric Chemistry and Physics*, 15(4), 2215-2224.

Ramboll Environ. 2016. User's Guide: Comprehensive Air Quality Model with extensions, Version 6.30. Available at http://www.camx.com.

Saiz-Lopez, A., J.M.C. Plane, A.R. Baker, L.J. Carpenter, R. Von Glasow, J.C. Gómez Martín, G. McFiggans, R.W. Saunders. 2012. Atmospheric chemistry of iodine. *Chem. Rev.*, 112, 1773–1804, doi:10.1021/cr200029u.

Smith, J.H., M. Estes, F. Mercado. 2014. Quantifying Regional Background Ozone for the Houston-Galveston-Brazoria Nonattainment Area. Presented at Midwest and Central States Air Quality Workshop, St. Louis, http://www.ladco.org/about/general/2014%20Midwest%20Air%20Quality%20Workshop/Presentations.html.

Smith, J. H., M. Estes, J. Mellberg, O. Nopmongcol, G. Yarwood. 2015. Addressing model over-prediction of ozone influx from the Gulf of Mexico. Presented at CMAS 2015, https://www.cmascenter.org/conference/2015/agenda.cfm.

Yarwood, G., J. Jung, U. Nopmongcol, C. Emery. 2012. Improving CAMx Performance in Simulating Ozone Transport from the Gulf of Mexico. Final Report for Work Order No. 582-11-10365-FY12-05.

Yarwood, G., T. Sakulyanontvittaya, U. Nopmongcol, B. Koo. 2014. Ozone Depletion by Bromine and Iodine over the Gulf of Mexico. Final Report for Work Order No. 582-11-10365-FY14-12 https://www.tceq.texas.gov/airquality/airmod/project/pj_report_pm.html.